10th anniversary themed issue for Journal of Materials Chemistry A

Supporting Information

High-quality single-walled carbon nanotube films as ultralight current collectors for flexible supercapacitors

Sheng Zhu, Zeyao Zhang,* Jian Sheng, Guodong Jia, Jiangfeng Ni,* and Yan Li*

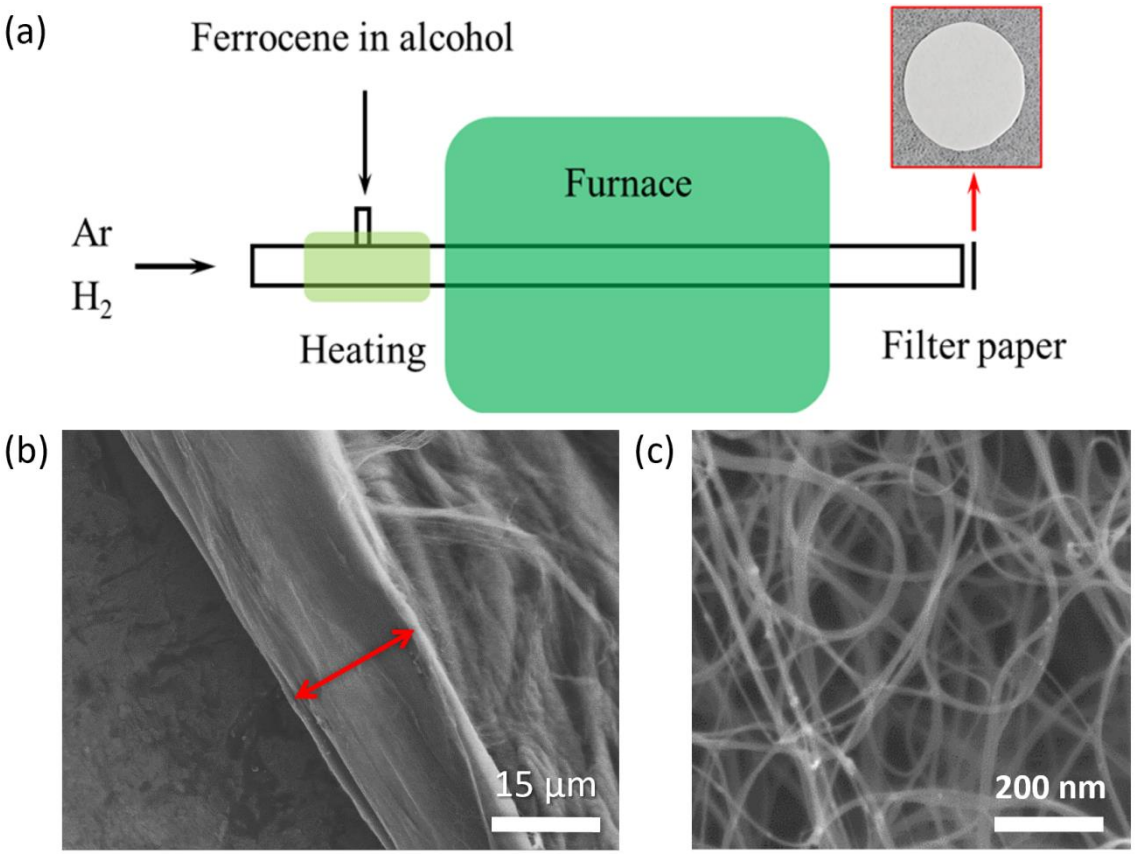

Figure S1. (a) Schematic experimental setup for synthetic process of the SWCNFs. (b) Cross-sectional SEM image of SWCNFs. (b) TEM image of SWCNFs.

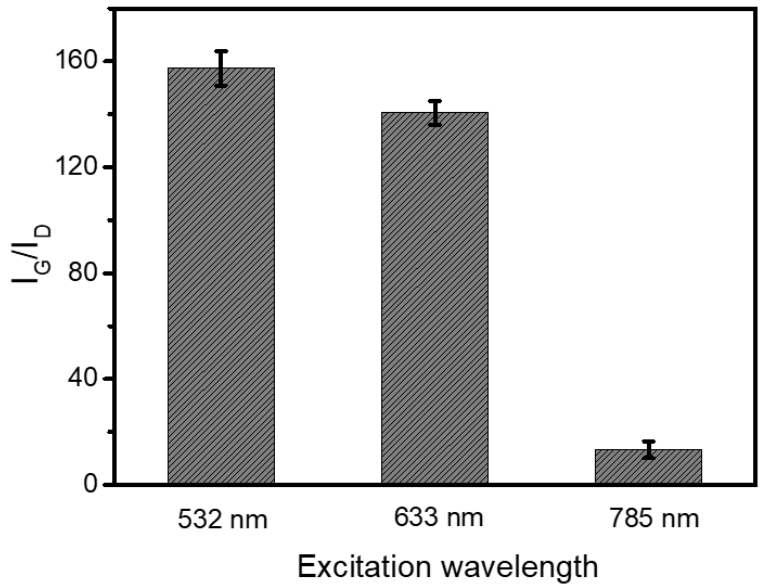

Figure S2. I_G/I_D values calculated from Raman spectra with the excitation wavelength of 532 nm, 633 nm and 785 nm.

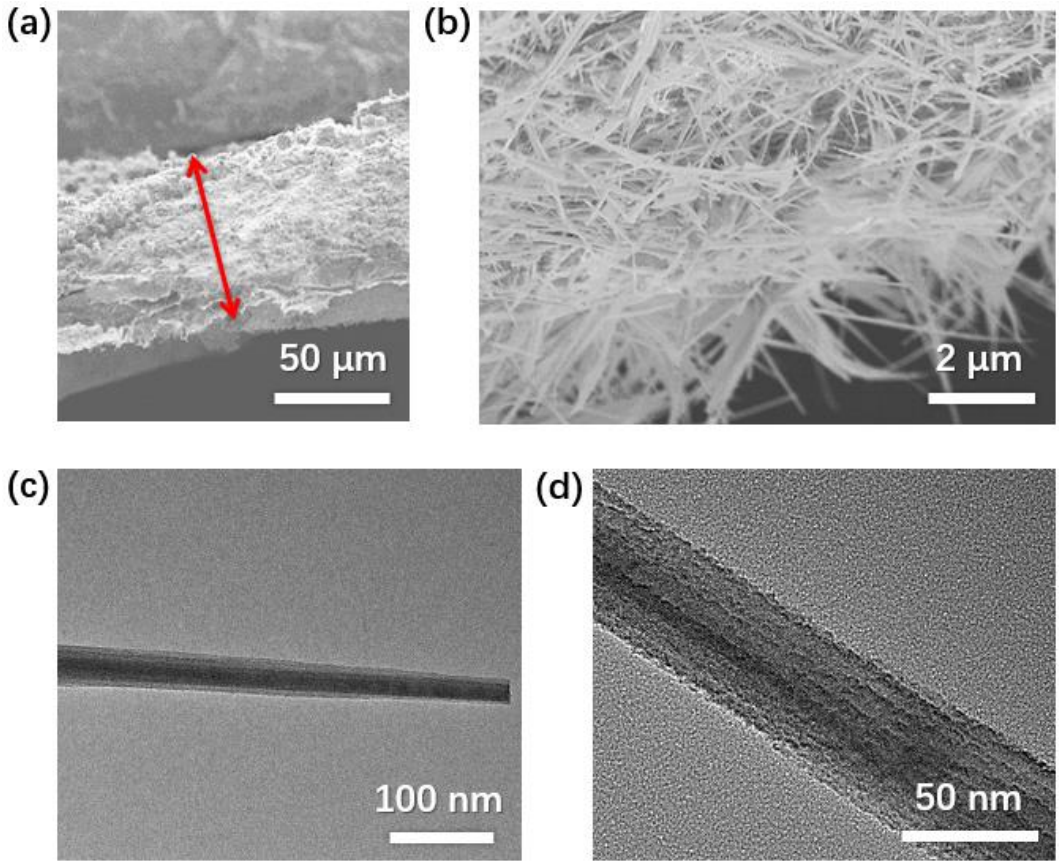

Figure S3. (a, b) Cross-sectional SEM images of SWCNF-CCH. (c, d) TEM images of a CCH nanowire. CCH: cobalt (II) carbonate hydroxide ($CO_2(OH)_2CO_3$)

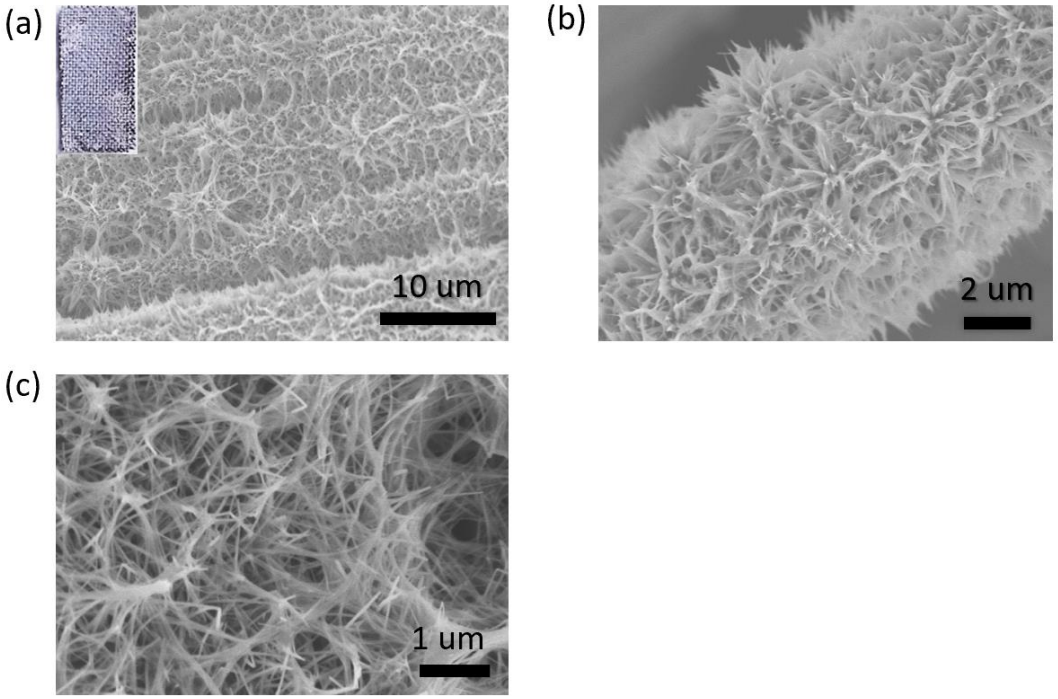

Figure S4. SEM images of carbon cloth-CCH.

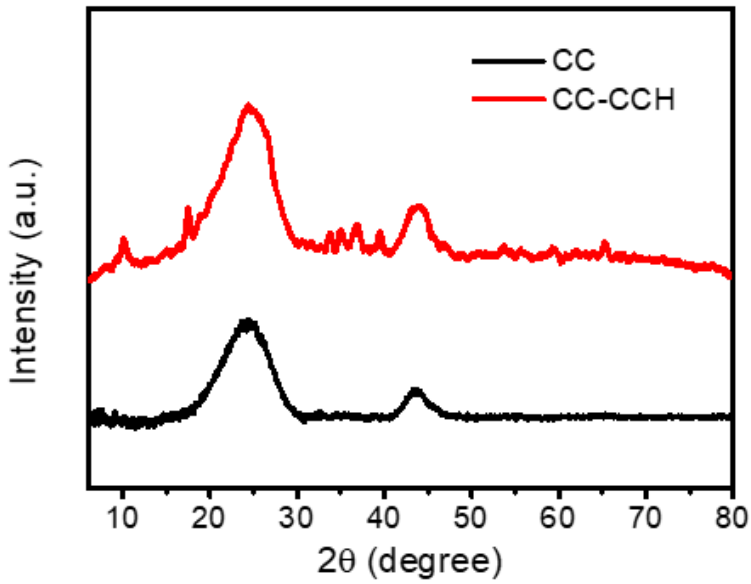

Figure S5. XRD of carbon cloth-CCH.

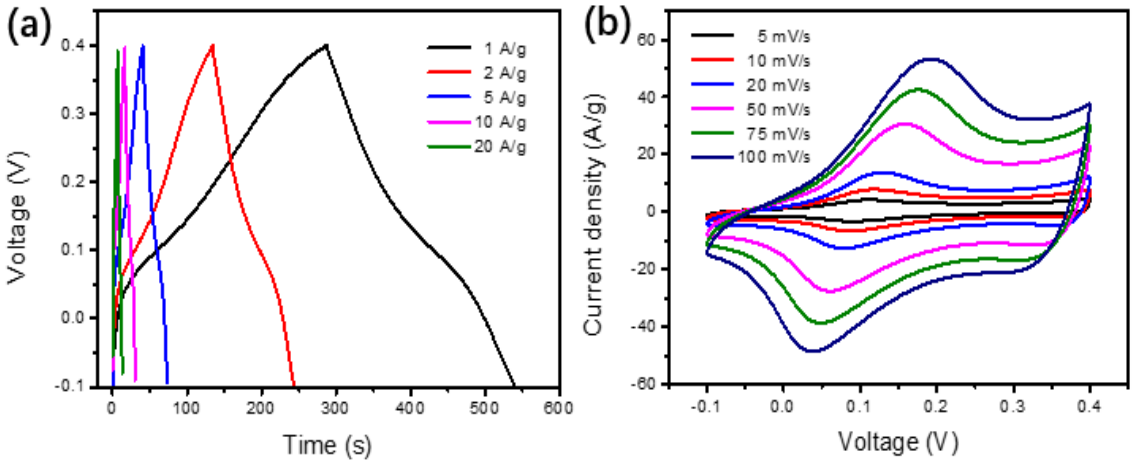

Figure S6. (a) GCD curves of carbon cloth-CCH under different current densities. (b) CV curves of carbon cloth-CCH at various scan rates.

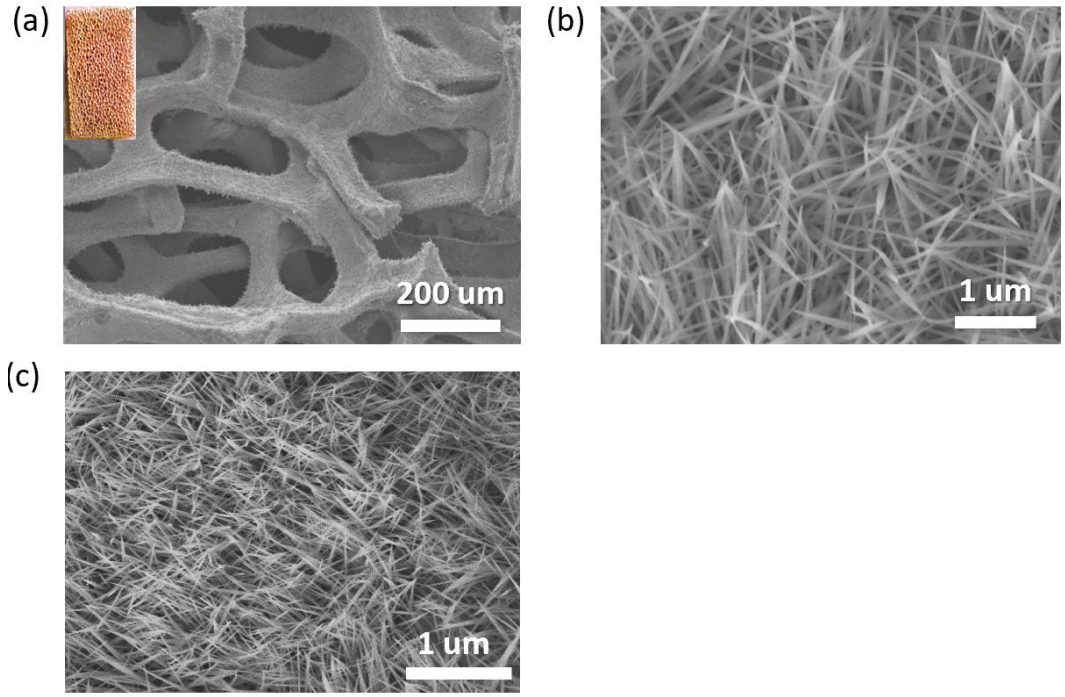

Figure S7. SEM images of Ni foam-CCH.

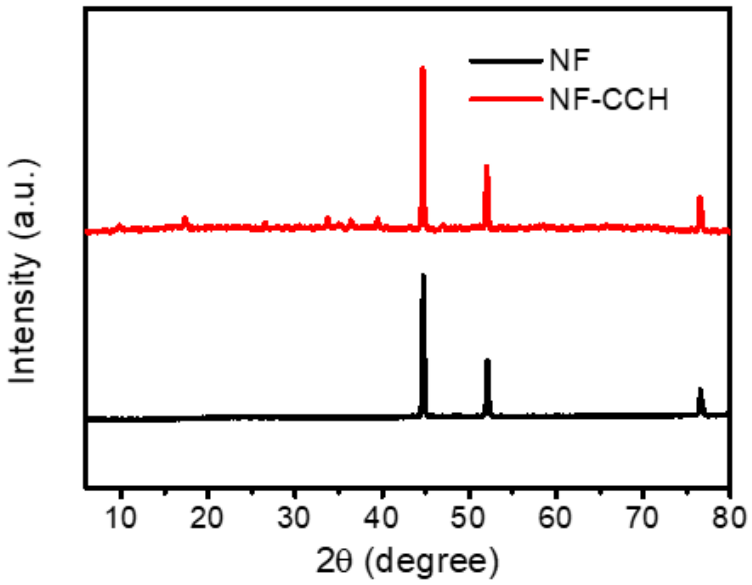

Figure S8. XRD of Ni foam-CCH.

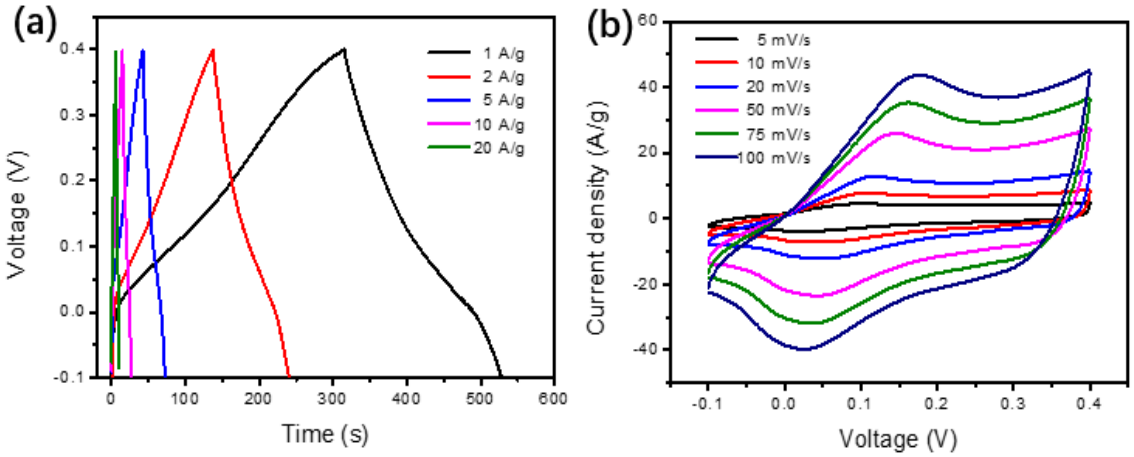

Figure S9. (a) GCD curves of Ni foam-CCH under different current densities. (b) CV curves of Ni foam-CCH at various scan rates.

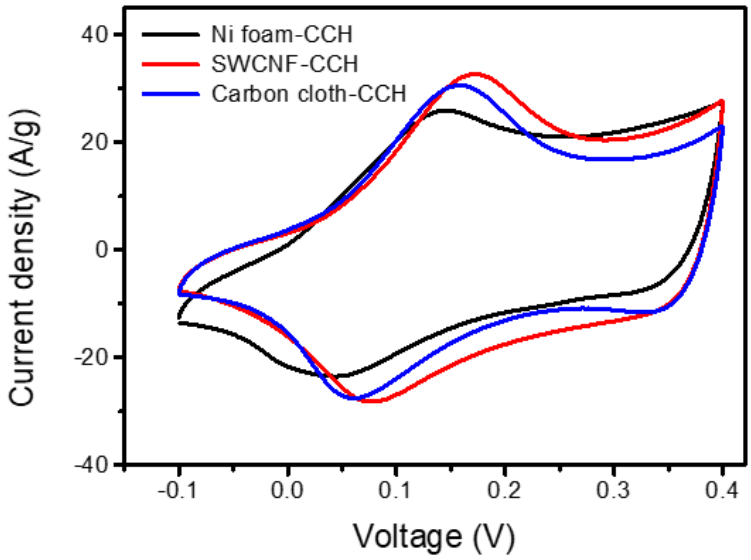

Figure S10. CV curves of CCH loaded on different current collectors.

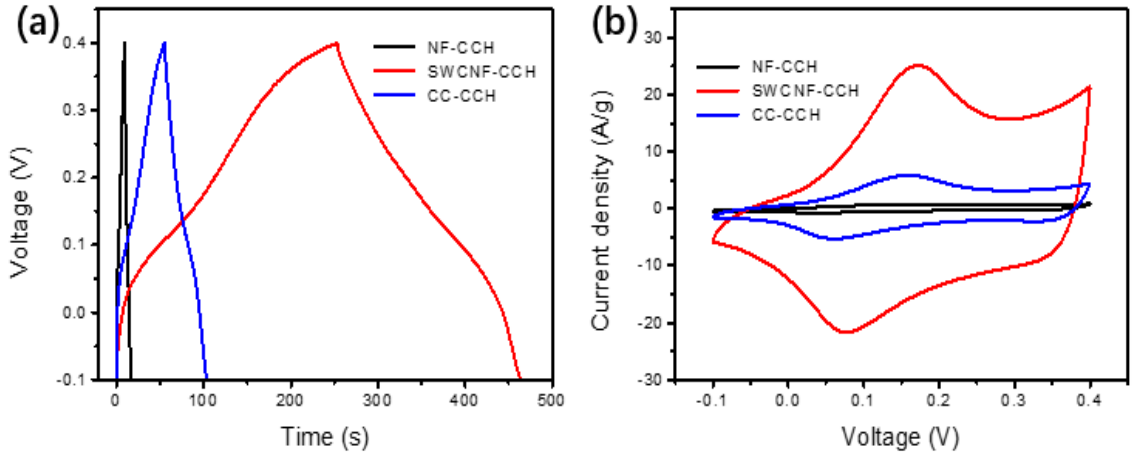

Figure S11. Consider the mass of CCH and current collectors. (a) GCD curves of CCH loaded on different current collectors. (d) CV curves of CCH loaded on different current collectors.

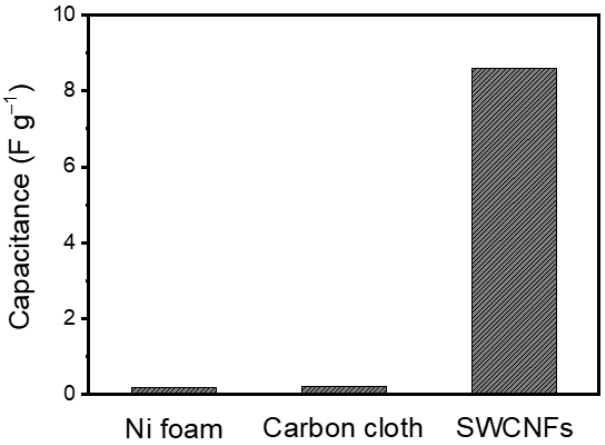

Figure S12. Specific capacitances of pure current collectors including Ni foam, carbon cloth, and SWCNFs.

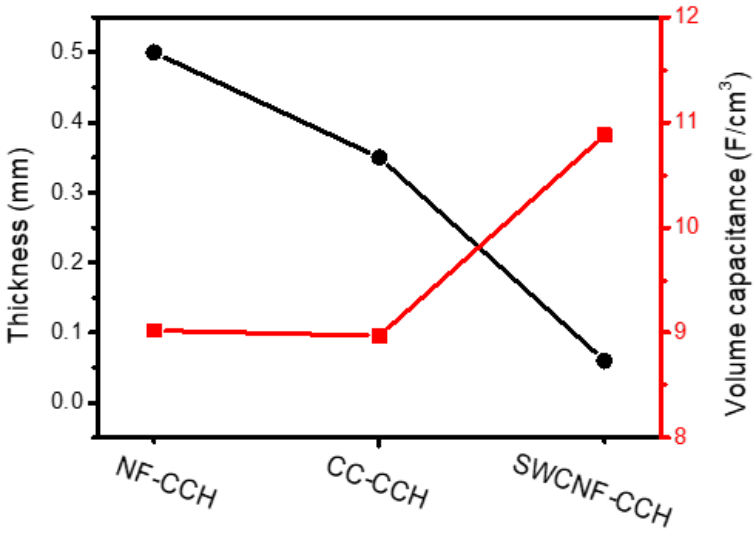

Figure S13. Thickness of different current collectors and the volume capacitance of CCH loaded on different current collectors when consider the total mass of CCH and current collectors.

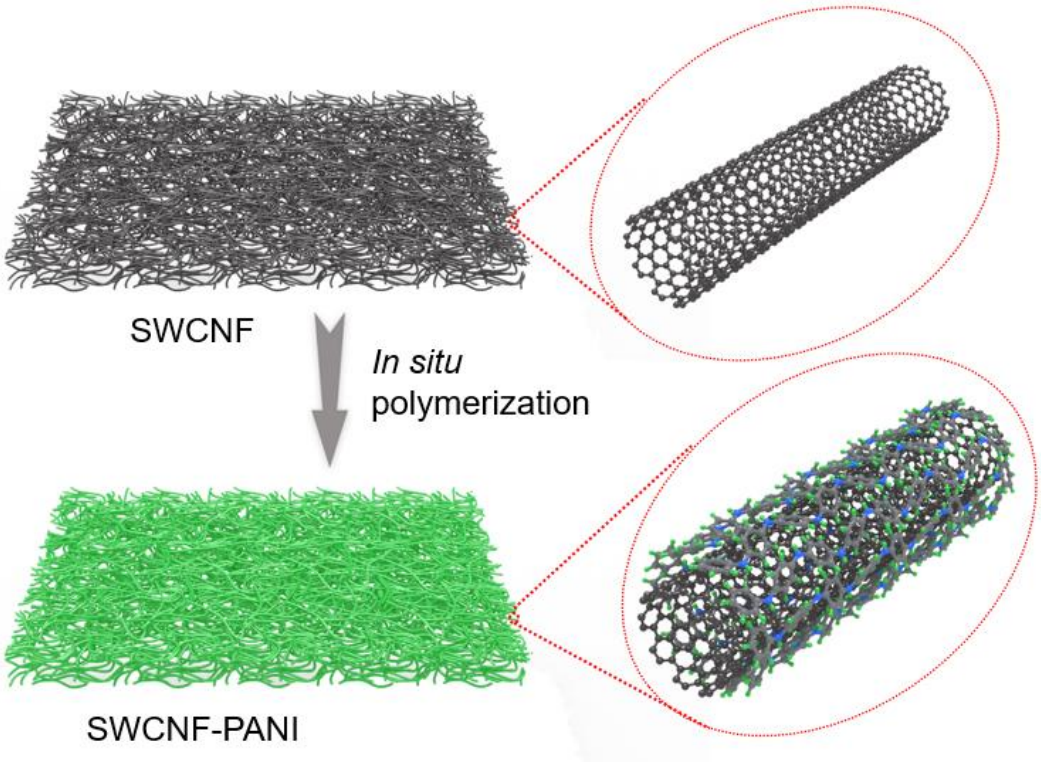

Figure S14. Schematic illustration for synthetic process of SWCNF-PANI.

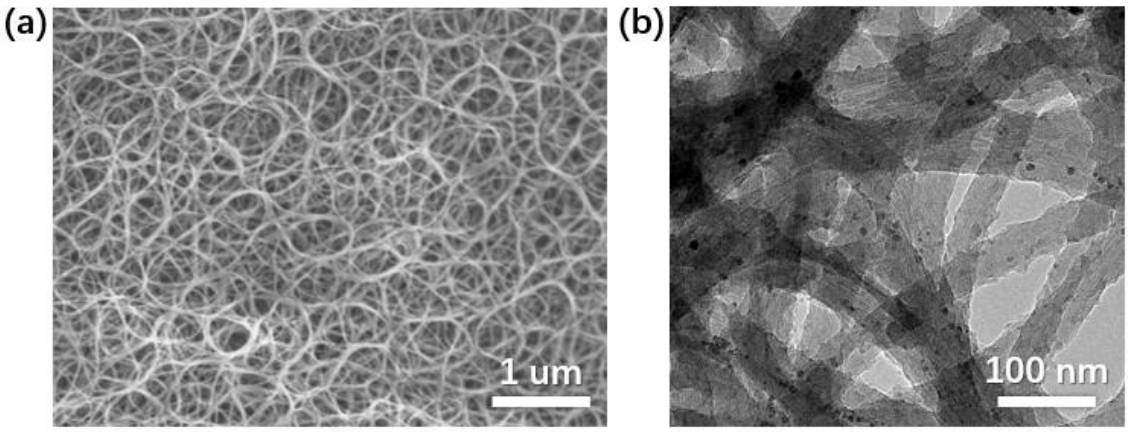

Figure S15. (a) SEM image of SWCNF-PANI. (b) TEM image of SWCNF-PANI.

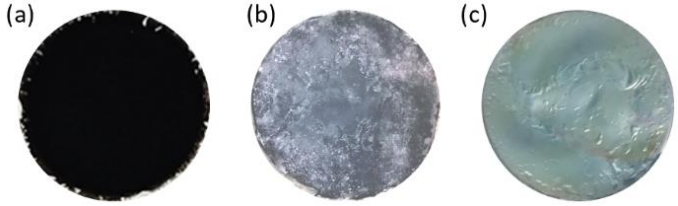

Figure S16. Optical images of SWCNT, SWCNT-$Co_2(OH)_2CO_3$ and SWCNT-PANI.

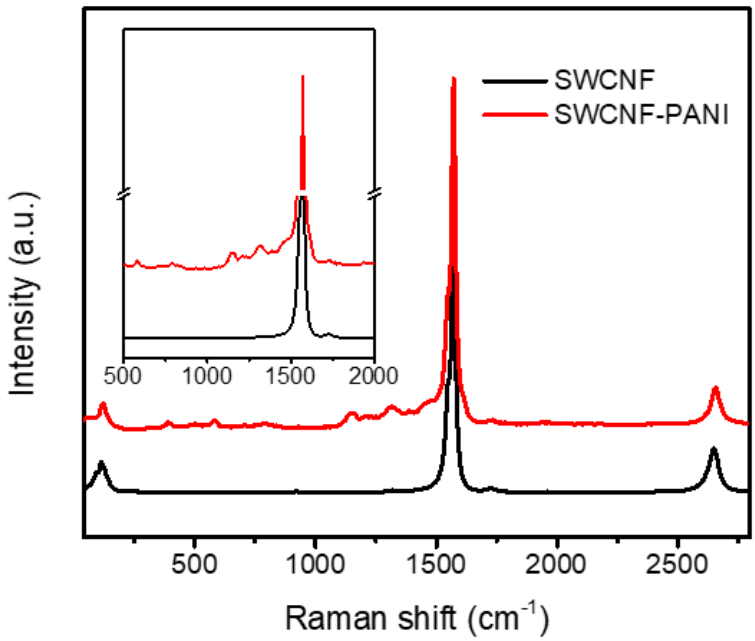

Figure S17. Raman spectrum of SWCNF and SWCNF-PANI.

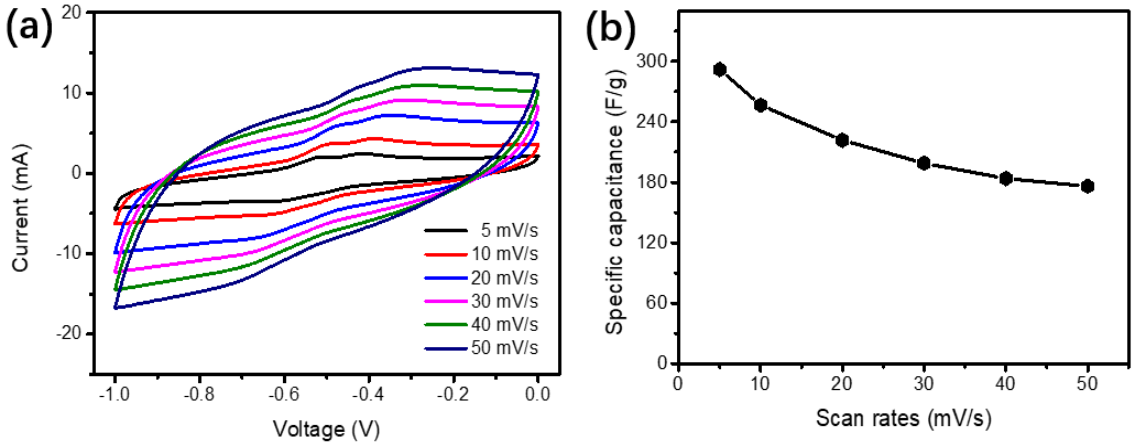

Figure S18. (a) CV curves of SWCNF-PANI. (b) Capacitance retention of SWCNF-PANI at various scan rates.

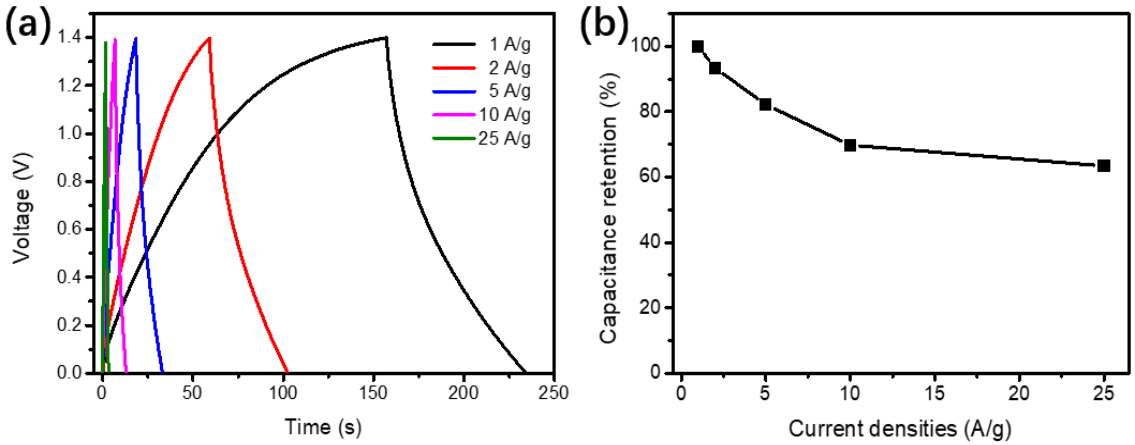

Figure S19. (a) GCD curves of SWCNF-CCH//SWCNF-PANI hybrid FSSCs. (b) Capacitance retention of SWCNF-CCH//SWCNF-PANI hybrid FSSCs at various scan rates.

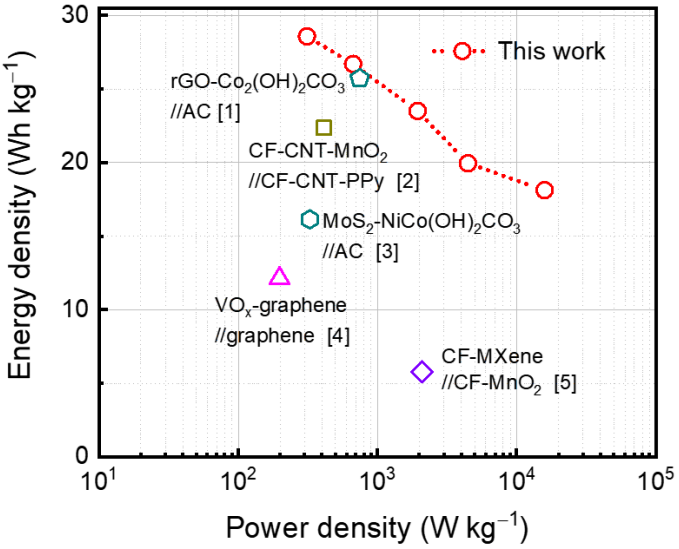

Figure S20. Comparison of Ragone plots of SWCNF-CCH//SWCNF-PANI hybrid FSSC with other reported devices.

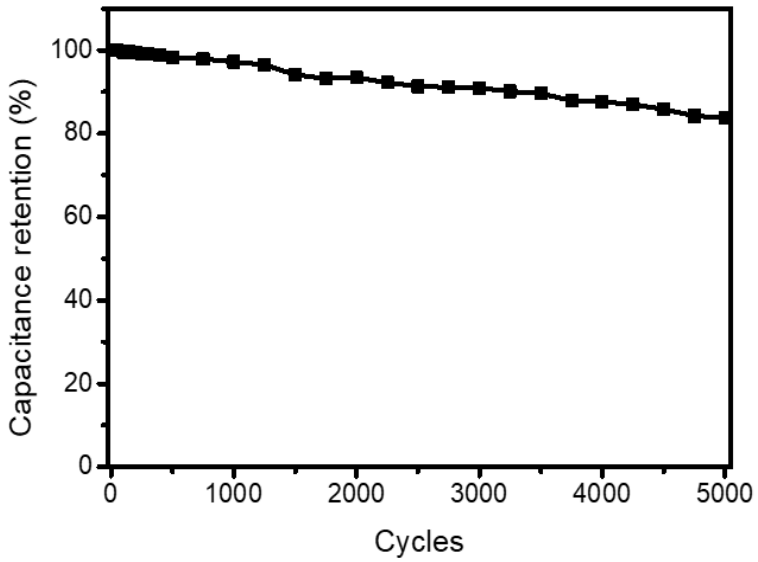

Figure S21. Cycling performance of SWCNF-CCH//SWCNF-PANI hybrid FSSCs.

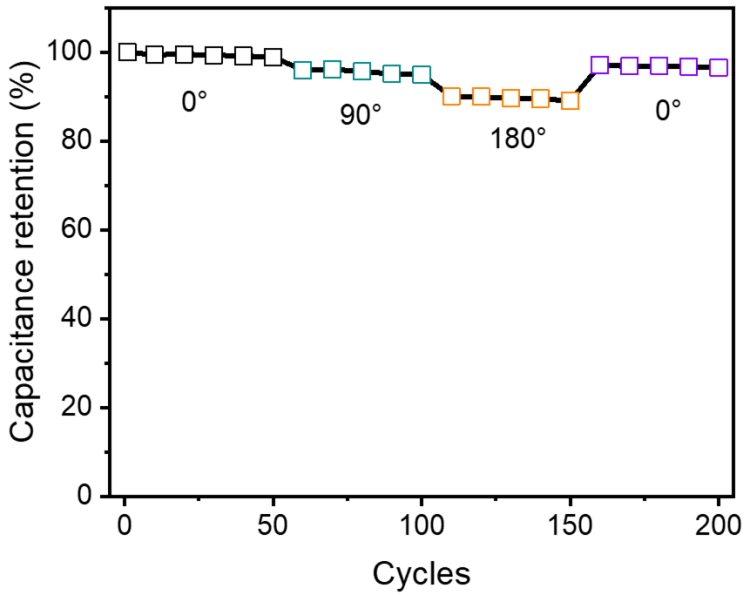

Figure S22. Cycling performance of SWCNF-CCH//SWCNF-PANI hybrid FSSCs under various bending conditions.

References

1. X. Leng, L. Wu, Y. Liu, C. Li, S. Wei, Z. Jiang, G. Wang, J. Lian and Q. Jiang, *J. Mater. Chem. A*, 2016, **4**, 17171-17179.

2. T. Cen, L. Chen, X. Zhang, Y. Tian, X. Fan, *Electrochim. Acta*, 2021, **367**, 137488.

3. A.Y. Chen, H.H. Liu, P. Qi, X.F. Xie, M.T. Wang and X.Y. Wang, *J. Alloy. Compd.*, 2021, **864**, 158144.

4. A.-Y. Wang, M. Chaudhary and T.-W. Lin, *Chem. Eng. J.*, 2019, **355**, 830-839.

5. Y. Wei, M. Zheng, W. Luo, B. Dai, J. Ren, M. Ma, T. Li and Y. Ma, *J. Energy Storage*, 2022, **45**, 103715.